

Objective Evaluation of Short-Crack Toughness Curves Using Indentation Flaws: Case Study on Alumina-Based Ceramics

Linda M. Braun,^{*,†} Stephen J. Bennison,^{*,‡} and Brian R. Lawn^{*}

Materials Science and Engineering Laboratory, National Institute of Standards and Technology,
Gaithersburg, Maryland 20899

An objective methodology is developed for evaluating toughness curves (*T*-curves) of ceramics using indentation flaws. Two experimental routes are considered: (i) conventional measurement of inert strength as a function of indentation load; (ii) in situ measurement of crack size as a function of applied stress. Central to the procedure is a proper calibration of the indentation coefficients that determine the *K*-field of indentation cracks in combined residual-contact and applied-stress loading, using data on an appropriate base material with single-valued toughness. Tests on a fine-grain alumina serve to demonstrate the approach. A key constraint in the coefficient evaluation is an observed satisfaction of the classical indentation strength–(load)^{−1/3} relation for such materials, implying an essential geometrical similarity in the crack configurations at failure. *T*-curves for any alumina-based ceramic without single-valued toughness can then be generated objectively from inert-strength or in situ crack-size data. The methodology thereby circumvents the need for any preconceived model of toughening, or for any prescribed analytical representation of the *T*-curve function. Data on coarse-grained aluminas and alumina-matrix material with aluminum titanate second-phase particles are used in an illustrative case study.

I. Introduction

TOUGHNESS curves or resistance curves (*T*-curves, *K_R*-curves, *R*-curves), which describe a functional dependence of toughness on crack size, are now known to have a profound influence on the mechanical properties of ceramics.^{1–3} Traditional *T*-curve measurements are made with long cracks in notched specimens. However, some of the most important mechanical properties, notably strength, are determined in the domain of short cracks, i.e., cracks on a scale comparable with that of the microstructure. As intimated in measurements of crack extension from natural^{4,5} and controlled^{6,7} surface flaws in several ceramics, the critical short-crack region of interest lies below the lower limits of valid extrapolation from long-crack data.

It is in this context that radial cracks from Vickers indentations have been widely used as a means for evaluating toughness properties in the short-crack region. In the most practical form of the method, inert strength is measured as a function of indentation load.^{8,9} Materials with single-valued toughness are characterized by a classical indentation strength–(load)^{−1/3} relation;⁸ the existence of a *T*-curve may then be inferred by departures

from this relation. Specifically, as the *T*-curve becomes more pronounced the strength tends to a weaker dependence on indentation load, and thence on initial flaw size.^{10,11} This quality of *flaw tolerance* is attributed to stabilization of crack growth from a shielding *K*-field that increases with crack extension¹ (or, alternatively, an *anti*-shielding *K*-field that *decreases* with extension^{1,10}), and is a desirable end result in structural design.

A second form of the indentation method entails piecewise measurement of radial crack extension under monotonically increasing applied loading, in much the same way as indicated above for natural flaws. This approach derives from early work on materials with single-valued toughness, notably soda–lime glass,⁸ aimed at quantifying the stabilizing role of residual contact stresses in the fracture mechanics. With the indentation *K*-field thus calibrated one should, in principle, be able to evaluate any *K*-field increment (or decrement) due to microstructural shielding. This approach has recently been used to generate *T*-curves for certain alumina,⁶ inhomogeneous (elongated grain) silicon nitride,¹³ and zirconia ceramics.¹⁴

The indentation technique has not been without detractors. The most critical suggest that the presumed flaw tolerance in the measured strength–load response is not due to an intrinsic *T*-curve at all, but is an artifact of the technique. A common argument is that the tendency for the strength to indentation-size independence simply denotes a natural flaw “cutoff” at low loads. This is despite meticulous attempts to confirm that the failures occur from indentation sites.¹¹ Another school points out that artifacts in both indentation–strength and applied-stress/crack-extension data can arise from crack-size variations in the two coefficients that determine the combined applied-stress plus residual-contact indentation *K*-field.^{12,13} Improper specification of those coefficients can result in *apparent T*-curves in materials which are unquestionably single-valued in toughness, including glass.¹² Yet other critics acknowledge the association of indentation–strength data with an underlying *T*-curve, but question the curve-fitting procedures used in quantitative deconvolutions of the latter from the former. Analyses based on specific microstructural shielding models,^{10,11,15,16} regardless of how well they might be substantiated by physical observation,^{17,18} typically require the specification of several adjustable microstructural parameters, some of which can be determined only from elaborate data fits. Slight variations in these adjustable parameters can significantly alter the characteristics of the deconvoluted *T*-curve. Conversely, procedures that represent the *T*-curve by simplistic empirical functions^{19–21} are open to objection for inconsistencies with physical reality. All such criticisms must be answered if indentation–strength is to be retained as a viable means of *T*-curve evaluation.

In light of this background, we endeavor here to establish a sound scheme for evaluating *T*-curves of ceramics *objectively* from indentation–strength and/or applied-stress/crack-extension data. We illustrate with results from previous indentation–strength studies on alumina-based ceramics, one on monophasic aluminas covering a wide range of grain sizes²² and the other on an alumina-matrix composite with aluminum titanate second-phase particles.²³ In the first of these earlier studies a detailed

K. T. Faber—contributing editor

Manuscript No. 196065. Received January 8, 1992; approved June 24, 1992.

Supported by the U.S. Air Force Office of Scientific Research, U.S. Office of Naval Research, and E. I. du Pont de Nemours and Co., Inc.

^{*}Member, American Ceramic Society.

[†]Guest Scientist from the Department of Materials Science and Engineering, Lehigh University, Bethlehem, PA 18015.

[‡]Now at E. I. du Pont de Nemours and Co., Wilmington, DE 19898.

fracture-mechanics grain–grain bridging model¹⁶ was used to deconvolute the T -curves. Those T -curves were found to deviate negligibly from the baseline toughness of alumina at the finest grain size (2.5 μm), but became progressively more pronounced with increasing coarsening. Here, we devise a much simpler methodology for generating the T -curves, without any need for specific models of the underlying shielding mechanism or for parametric deconvolutions. Our evaluation centers around an appropriate determination of the two coefficients that quantify the indentation K -field. We ensure self-consistency in this determination by noting that the ideal indentation strength–(load)^{-1/3} relation is well satisfied for the finest grain-size (control) alumina, and use this relation to constrain the two coefficients. An integral part of our strategy is the use of in situ observations of crack growth during stressing to failure, to obtain essential information on the indentation–crack dimensions. These in situ observations reinforce our previous contention that failure does indeed occur from indentation sites, enable explicit calibration of the indentation coefficients, and (in favorable cases) provide an alternative route to evaluation of the T -curves.

II. The Problem of Analytically Deconvoluting T -Curves from Indentation Data

Let us consider how one might objectively determine the T -curve from indentation–strength and applied-stress/crack-extension data. Begin with the general relation for the “crack-tip” K -field as a function of radial crack size c relative to the contact center for equilibrium indentation cracks with residual deformation fields in a material with T -curve behavior:^{1,2,11,16}

$$K_A(c) = K_A + K_R + K_\mu \\ = \psi\sigma_A c^{1/2} + \chi P/c^{3/2} + K_\mu(c) = T_0 \quad (1a)$$

K_A is the stress-intensity factor associated with the applied stress σ_A , K_R with the residual contact field at indentation load P , and K_μ with microstructural shielding (the source of the T -curve); ψ is a geometrical coefficient that characterizes the pennylike crack configuration;² $\chi \propto (E/H)^{1/2}$ is a coefficient, ideally independent of c , that characterizes the intensity of the residual field in terms of indentation hardness H and Young’s modulus E ;^{24,25} T_0 is a baseline toughness, *monocrystal* for transgranular fracture and *grain boundary* for intergranular fracture. Equation (1a) may be normalized to

$$K_A/T_0 = (\psi/T_0)\sigma_A c^{1/2} + (\chi/T_0)P/c^{3/2} + K_\mu/T_0 = 1 \quad (1b)$$

For materials with no T -curve, $K_\mu = 0$. For materials with T -curve, $K_\mu \neq 0$, but in this study we make absolutely no statement as to what explicit functional form $K_\mu(c)$ might take. Equation (1a) may be transposed into a form appropriate to a “global” K -field

$$K'_A(c) = \psi\sigma_A c^{1/2} + \chi P/c^{3/2} \\ = T_0 - K_\mu(c) = T_0 + T_\mu(c) = T(c) \quad (2)$$

where $K'_A(c)$ is an effective applied stress-intensity factor, $T_\mu(c) = -K_\mu(c)$ is a shielding toughness term, and $T(c)$ defines the T -curve for the material.^{1,2}

Equation (2) may be solved for the applied stress as a function of equilibrium crack size:

$$\sigma_A(c) = (1/\psi c^{1/2})[T(c) - \chi P/c^{3/2}] \quad (3)$$

Generally, because of the stabilizing influence of $K_R(c)$ and $K_\mu(c)$ in Eq. (1), the newly formed indentation cracks will extend stably prior to crack failure, so the critical failure configuration does *not* identify with spontaneous propagation from the initial crack size, c_0 .^{1,8} The inert strength identifies with the critical configuration $\sigma_A = \sigma_M$, $c = c_M > c_0$, at which $\sigma_A(c)$ passes through a dominant maximum, corresponding to a “tangent condition”

$$dK'_A(c)/dc = dT(c)/dc \quad (4)$$

in Eq. (2).^{1,2}

Since the explicit mathematical form of $T(c)$ is not specified a priori here, analytical solutions of the strength function $\sigma_M(P)$ for materials with T -curves are not generally obtainable from Eq. (3). (In fact, analytical solutions are not guaranteed even when the form of $T(c)$ is specifiable.) On the other hand, if the coefficients ψ and χ can be properly calibrated from $\sigma_A(c)$ data on a control material with single-valued toughness, the T -curve should, in principle, be calculable directly from Eq. (2).

III. Experimental Procedure

The basis of the experimental T -curve determinations is the analysis of inert strength data for specimens with indentation flaws, in combination with in situ measurements of the flaw evolution to failure. Here we use strength data from earlier studies,^{22,23} but include a brief description of the test procedure for completeness. A description of the in situ crack-extension measurements is given in more detail.

(1) Materials

Alumina was chosen as a base for this study because of its extensive adoption as a model polycrystalline material in several previous indentation studies, as well as its common use as a practical ceramic. The starting material was a high-purity (500 at. ppm Mg/Al) alumina with equiaxed grains of mean grain size 2.5 μm .²² At this fine grain size, alumina has a negligible T -curve,²² and so serves as a convenient *control* for the materials described below. Specimens were machined into disks of thickness 3 mm.

Aluminas with significant T -curves were produced by heat-treating batches of the starting material to produce microstructures with enlarged grain sizes.²² Here we consider grain sizes 15, 35, and 80 μm .

An alumina-matrix composite with especially pronounced flaw tolerance²³ was also investigated. This composite contains 20 vol% aluminum titanate as a second phase. Preparation was by sintering, via a conventional powder processing route.^{26,27} The mean size of the matrix alumina and aluminum titanate grains was 6 μm , but with occasional agglomerates of the latter of 5 to 10 grains.²³ Specimens of this material were cut into disks 5 mm thick.

All specimens were polished on one side to remove spurious machining stresses, and to observe ensuing indentation cracks with minimum surface obstruction.

(2) Indentation–Strength Tests

Vickers indentations at specified loads were made in the center of each polished surface. The disks were broken in biaxial flexure, indentations centered on the tensile side, with 6-mm-diameter flat loading on three-ball support.²⁸ These tests were conducted with a drop of oil on the indentation site and broken in fast loading (within 10 ms), to maintain “inert” conditions. Stresses at the indentation site were calculated from the applied load using thin plate theory.²⁸ Post-mortem examinations were made of all polished specimens to confirm failure initiation from the indentation sites.

Some comparative tests were made on specimens with annealed indentations, to remove the crack-stabilizing influence of the contact field.⁸

(3) In Situ Observations of Crack Extension

In situ observations of indentation-crack growth to failure were made using a custom-built biaxial flexure fixture for placement on an optical microscope or in an SEM. A schematic is shown in Fig. 1. A piezoelectric translator was used to apply a load to the biaxial flexure specimen. Stable growth of the surface radial cracks could then be followed directly as a function of monotonically increasing load, measured using a load cell. Quantitative tests were carried out exclusively on the optical

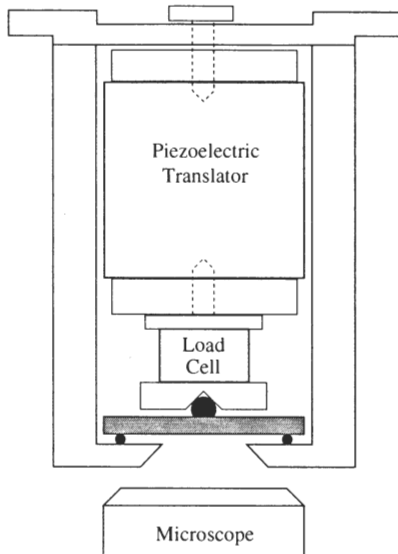


Fig. 1. Schematic of fixture for viewing indentation crack growth in situ during stressing to failure. Load is delivered to a biaxial flexure specimen by a piezoelectric translator and is measured by a load cell. The fixture can be located on the stage of an optical microscope or in an SEM.

microscope. Indentation sites were again covered with oil to reduce the influence of moisture, and covered with a glass cover slide to facilitate microscopic observation. In our tests a typical run to failure took ≈ 1 – 2 h. Crack sizes were measured at each stage of loading from video recordings of the crack evolution after failure was complete. Subsidiary observations were made in the SEM on the alumina-matrix composite to examine the crack-face morphology.

The immediate postindentation crack patterns in the fine-grain control alumina and the alumina-matrix composite were observed to be "well-developed," i.e., four radial arms extending symmetrically from the indentation corners, with each arm of length more than twice the Vickers impression half-diagonal.²⁹ Such was not the case for the coarsest aluminas, where the cracks deflected abruptly along local crack grain boundary facets in a more irregular fashion. In situ observations on the coarse aluminas were accordingly confined to semiquantitative estimates of the net crack extension to failure.¹⁷

(4) Hardness and Modulus

The indentation hardness (load/projected contact area) was evaluated directly from the impression diagonals of the Vickers indentations for each material. Young's modulus for the alumina was taken from a previous estimate,²⁹ and for the composite material determined by an independent acoustic technique.³⁰

IV. Results and Analysis

(1) Indentation-Strength Data

Figure 2 is a plot of inert strength vs indentation load results for our as-indentated 2.5- μm -grain-size control alumina, from an earlier study.²² Figure 3 is a plot of corresponding results for 15, 35, and 80 μm for the coarse-grain test aluminas, from the same data source. All data points with error bars are means and standard deviations (logarithmic coordinates) for a minimum of four specimens at each prescribed load. These points exclusively represent confirmed failures from indentation sites. Any breaks away from indentations are included in a data pool for natural flaws, indicated at left by the shaded regions. Included in the plot for the control material in Fig. 2 are some additional individual results from the in situ runs (see Section IV(2)). The solid line in Fig. 2 is a least-squares data fit, in accordance with

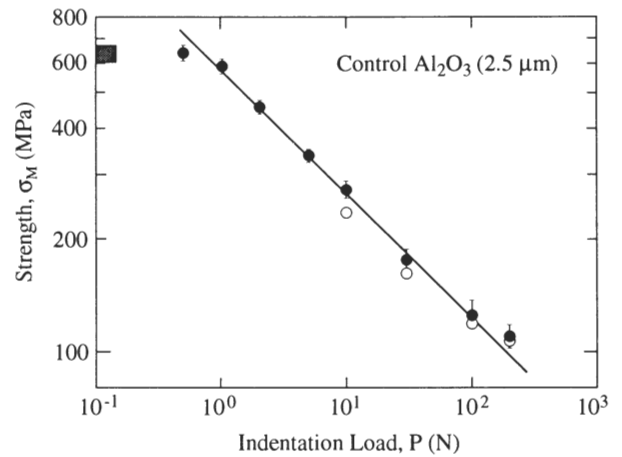


Fig. 2. Plot of $\sigma_M(P)$ inert strength data for control alumina, grain size 2.5 μm , with Vickers indentation flaws (closed symbols). Data from Ref. 22. Additional results from current individual in situ runs (open symbols). Solid straight-line fit of $(\text{slope})^{-1/3}$ (logarithmic coordinates) allows determination of $(T_0/\psi)(T_0/\chi)^{1/3}$ in Eq. (6b) for alumina.

prediction for a material with single-valued toughness (Section IV(2)). This last fit is reproduced in Fig. 3 (dashed lines) as a reference baseline for evaluating flaw tolerance in the coarser aluminas.

Figure 4 is a plot of corresponding inert strength vs indentation load results for the as-indentated alumina-matrix/aluminum titanate composite.²³ In this case data points with error bars are means and standard deviations for 4–10 specimens at each prescribed load. Again, the dashed line is reproduced from Fig. 2 as a reference baseline.

The results in Figs. 3 and 4 indicate large matrix grains and second-phase particles as important microstructural elements contributing to high flaw tolerance.³¹ We note the especially low sensitivity of the data to indentation load for the composite material in Fig. 4, i.e., enhanced strength at large P (approaching the long-crack region), counterbalanced by diminished strength at small P (short-crack region).

(2) In Situ Measurements of Crack Growth in Control Fine-Grain Alumina

As indicated earlier, the 2.5- μm -grain-size alumina was used as a control material for calibrating indentation coefficients. The indentations in this material were characterized by a well-formed radial crack system at each of the indentation loads P , with all four radial arms from the indentation corners equal in length to within 10% and with the radial surface traces exceeding twice the indentation half-diagonals (conditions for "well-developed" radial cracks²⁹). The fracture was predominantly intergranular.

On application of an applied flexural stress σ_A the radial cracks in the as-indentated ($\chi \neq 0$) specimens began to extend stably, but with discrete jumps in increments of one to three grains. Some persistent slow crack growth was observed at sustained stress after such jumps. After each such jump the load was ramped up until the next jump occurred. This piecewise extension proceeded relatively uniformly in all four radial directions until, at $\approx 80\%$ of the failure stress, one pair of cracks began to develop at the expense of the other. Radial crack sizes $2c$ were measured at initial and final extremities of this dominant pair at each abrupt jump-arrest point. Figure 5 is a plot of the $\sigma_A(c)$ data for several values of P . Such precursor stable growth has been well documented in silicate glasses,⁸ homogeneous silicon nitride,³² and other fine-grain ceramics.

Let us now examine $\sigma_A(c)$ in Eq. (3) for the special case of a single-valued toughness, $T = T_0$. For inert environment it is readily shown⁸ for this case that the crack begins stable growth from its immediate postindentation configuration at

$$\sigma_A = 0 \quad (5a)$$

$$c = c_0 = (\chi P/T_0)^{2/3} \quad (5b)$$

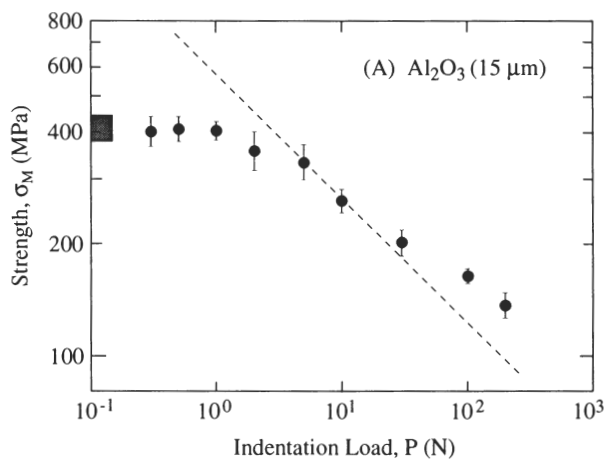
to instability at the maximum ($d\sigma_A/dc = 0$)

$$\sigma_A = \sigma_M = (3T_0/4\psi)(T_0/4\chi P)^{1/3} \quad (6a)$$

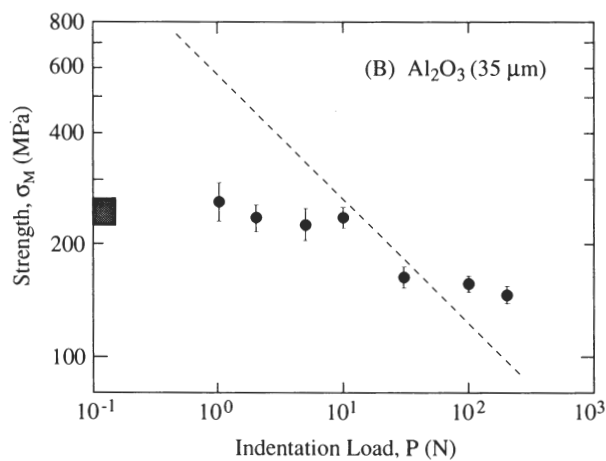
$$c = c_M = (4\chi P/T_0)^{2/3} \quad (6b)$$

Thus we have a stable branch of relative size $c_M/c_0 = 4^{2/3} = 2.52$. Constancy of the experimental quantity $\sigma_M P^{1/3}$ implies invariance in the compound parameter $\psi\chi^{1/3}$ with P at failure; similarly, constancy in $c_M P^{-2/3}$ implies invariance in χ . Using σ_M and c_M in Eq. (6) as normalizing parameters, Eq. (3) may be reduced to the universal function

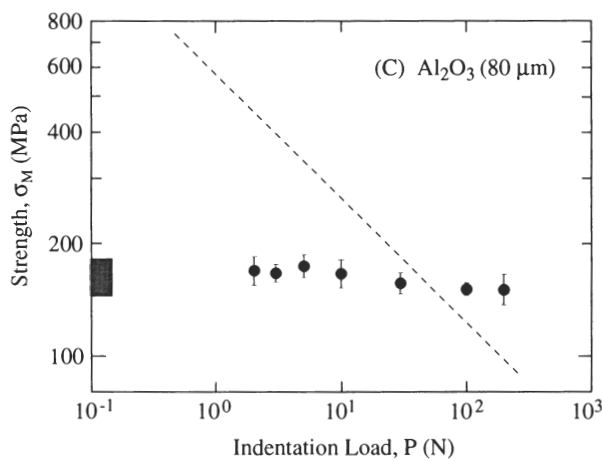
$$\sigma_A/\sigma_M = (1/3)(c_M/c)^{1/2}[4 - (c_M/c)^{3/2}] \quad (7)$$



(A)



(B)



(C)

Fig. 3. Plot of $\sigma_M(P)$ inert strength data for coarse-grain test aluminas with Vickers indentation flaws.²² Grain size: (A) 15, (B) 35, and (C) 80 μm . Fit to control data in Fig. 2 is reproduced as the dashed lines. Note higher flaw tolerance at larger grain size.

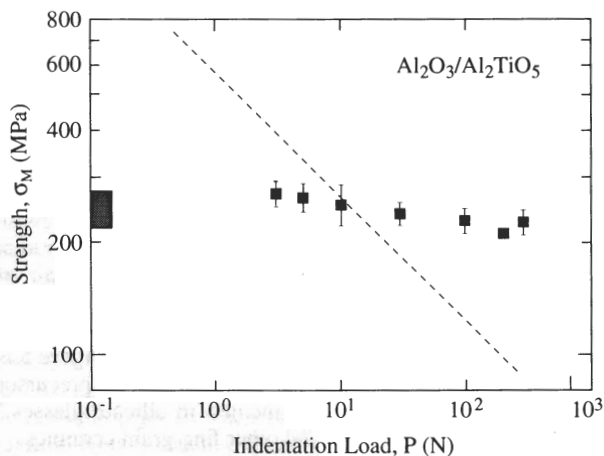


Fig. 4. Plot of $\sigma_M(P)$ inert strength data for aluminum titanate/alumina-matrix composite with Vickers indentation flaws. Dashed line is fit to 2.5- μm alumina control from Fig. 2.

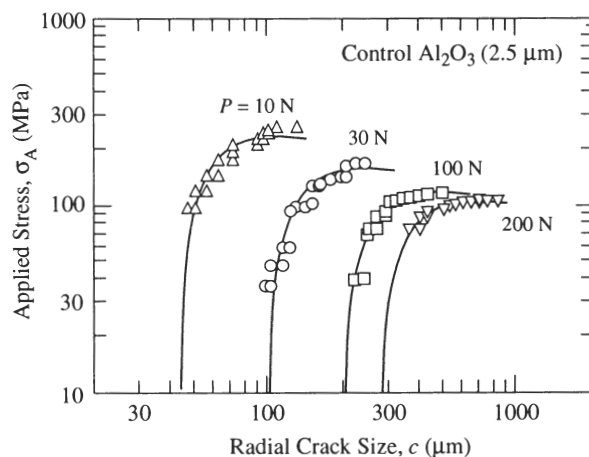


Fig. 5. Plot of in situ Vickers radial crack growth $\sigma_A(c)$ data (logarithmic coordinates) for 2.5- μm -grain-size alumina control, at specified values of P . Solid curves are fit to Eq. (3) at $T = T_0$ using calibrated coefficients from Section IV(3).

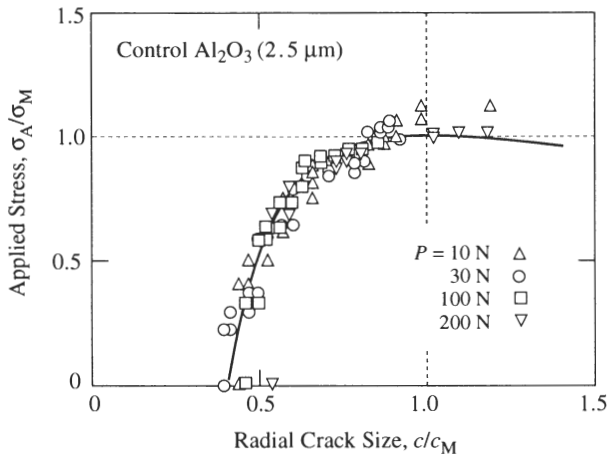


Fig. 6. Universal $\sigma_A(c)$ diagram (linear coordinates) for alumina control, Eq. (7), using collapsed data from Fig. 5. Fit allows determination of σ_M and c_M at each load P .

for materials with single-valued toughness.

In Fig. 6 we fit the data from Fig. 5 to this universal function by least-squares best-fitting values of σ_M and c_M at each load P . Note that this procedure makes full use of all the $\sigma_A(c)$ data, and does not rely exclusively on estimates of the actual maximum configuration.

(3) Calibration of Indentation Coefficients for Alumina-Based Systems

The quantities σ_M and c_M in Eq. (6) for as-indented specimens are most conveniently represented as functions of the independent test variable P . The $\sigma_M(P)$ evaluations from Fig. 6 are included in Fig. 2, to demonstrate overlap with the earlier inert strength results for the control alumina. In accordance with Eq. (6a), a best-fit to the data in Fig. 2 yields

$$\sigma_M P^{1/3} = 572.5 \pm 49.0 \text{ MPa} \cdot \text{N}^{1/3} \quad (8a)$$

Similarly, Fig. 7 is a plot of $c_M(P)$, and a best-fit to Eq. (6b) yields

$$c_M P^{-2/3} = 23.1 \pm 2.3 \text{ } \mu\text{m} \cdot \text{N}^{-2/3} \quad (8b)$$

Inserting the values from Eq. (8) back into Eq. (6), we evaluate

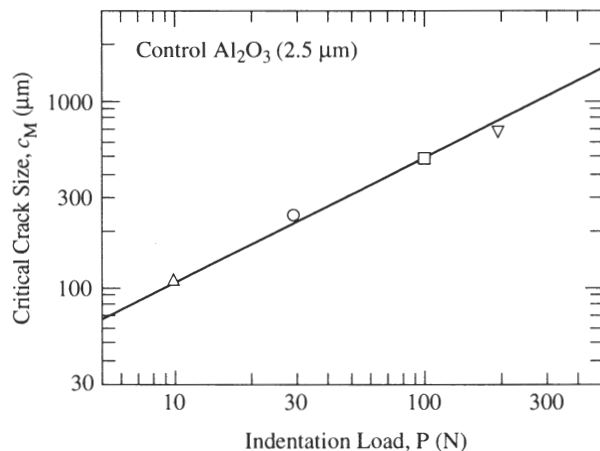


Fig. 7. Plot of c_M vs $P^{2/3}$ for alumina control. Fit allows determination of χ/T_0 in Eq. (6b).

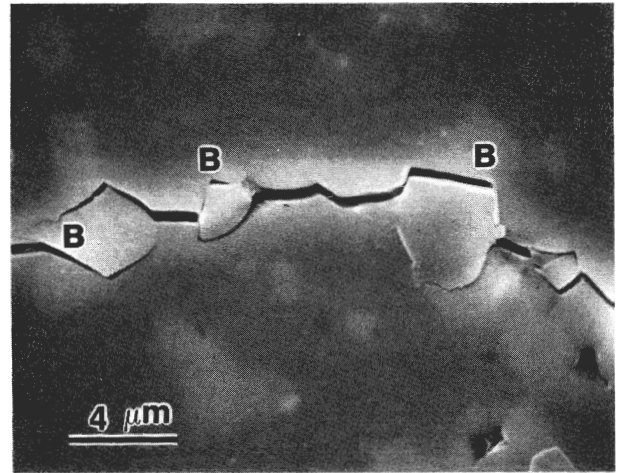


Fig. 8. SEM micrograph showing bridging in alumina-matrix composite. Aluminum titanate is light phase. B marks grain-grain bridge sites.

$$T_0/\chi = 36.0 \pm 3.6 \text{ MPa} \cdot \text{m}^{1/2} \quad (9a)$$

$$T_0/\psi = 3.68 \pm 0.34 \text{ MPa} \cdot \text{m}^{1/2} \quad (9b)$$

which, once T_0 is specified, provides us with “calibrated” indentation coefficients χ and ψ for our alumina.

Results from comparative tests on *postindentation-annealed* ($\chi = 0$) control alumina specimens allow a check on this calibration. In those tests failure occurred spontaneously from the initial flaws. Inserting $\sigma_A = \sigma_0$, $c = c_0$ into Eq. (3) at $T = T_0$, we obtain the critical stress

$$\sigma_A = \sigma_0 = (T_0/\psi c_0)^{1/2} \quad (10)$$

Measurements of σ_0 and c_0 from 13 specimens over the indentation load range $P = 0.2$ to 200 N give $\sigma_0 c_0^{1/2} = 1.77 \pm 0.22 \text{ MPa} \cdot \text{m}^{1/2}$, corresponding to $T_0/\psi = 2.82 \pm 0.36 \text{ MPa} \cdot \text{m}^{1/2}$. This value is somewhat lower than that in Eq. (9b), suggesting that ψ , while invariant with P at the critical configuration (as implied by the strength-(load)^{1/3} fit in Fig. 2), may well be a diminishing function of c in its evolution to failure.

(4) In Situ Observations of Crack Growth in Coarse-Grain Aluminas and Alumina-Matrix/Aluminum Titanate Composite

As indicated in Section III(3), the indentations in the coarse-grain monophase aluminas showed considerably more irregular geometry than in the fine-grain control alumina. Explicit determination of $\sigma_A(c)$ curves of the kind plotted in Fig. 5 was therefore not undertaken for the coarse-grain aluminas. On the other hand, in line with previous observations,¹⁷ the extent of stable crack growth prior to failure was observed to be substantially greater than the factor $c_M/c_0 = 2.52$ from Eqs. (5b) and (6b) for material of single-valued toughness, indicative of a shielding K -field.

For alumina-matrix/aluminum titanate composite, the relatively fine grain size produced reasonably well-defined radial crack patterns. Even so, some of the radial crack arms were larger than their neighbors. Especially strong deflections, presumably enhanced by strong *tensile* thermal expansion mismatch stresses,²⁶ occurred at alumina-matrix/aluminum titanate interphase boundaries (Fig. 8). The presumption of such tensile stresses was reinforced by the appearance of sporadic microcracking through the bulk of the composite material.^{26,27,31} Countervailing *compressive* stresses at adjacent interphase facets augment frictional grain-grain contacts at the separating crack walls, thereby creating effective bridges and contributing to a shielding K -field.^{16,23}

Quantitative in situ measurements of crack size as a function of applied stress were thereby made on composite specimens

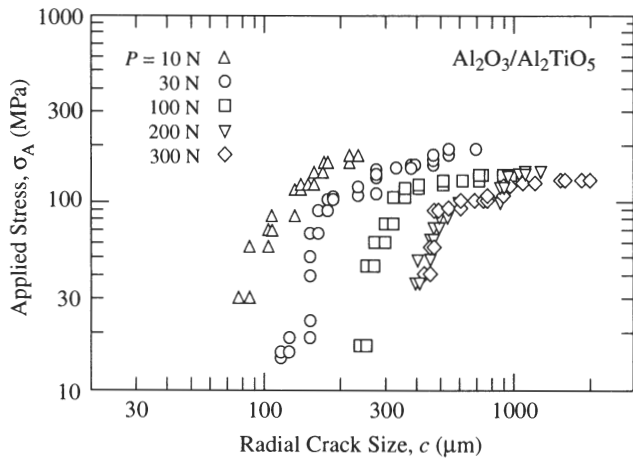


Fig. 9. Plot of $\sigma_A(c)$ in situ crack growth data for the aluminum titanate/alumina-matrix composite, at $P = 10, 30, 100, 200, 300$ N. Comparison with data for alumina fine-grain control at same loads (Fig. 5) shows much enhanced stable growth to failure in the composite, indicating an additional shielding K -field term.

indented at loads $P = 10, 30, 100, 200,$ and 300 N. Crack extension was more erratic than in the fine-grain alumina control, with jumps of several grain dimensions during steady loading. Persistent slow growth after such jumps was noticeably more pronounced than in the control alumina. Where the crack pattern was asymmetrical, the longer of two pairs of radial arms was measured. Figure 9 shows the ensuing $\sigma_A(c)$ data.

It is instructive to compare the data sets for the composite in Fig. 9 with those for the fine-grain alumina control material in Fig. 5. Observe first that the strength of the composite is relatively insensitive to indentation load, in accordance with Figs. 4 and 2. At the same time, the crack extension to failure at any given load is strongly enhanced. Such departures from the classical (Griffith) flaw response are indicative of a substantial stabilizing contribution to the K -field from the second phase.

(5) Modulus/Hardness Ratio

The modulus/hardness ratio for the base alumina material was determined as $E/H = (395 \pm 10 \text{ GPa})/(18.6 \pm 1.0 \text{ GPa}) = 21.3 \pm 1.7$, independent of grain size. The corresponding ratio for the alumina-matrix/aluminum titanate composite was $E/H = (300 \pm 25 \text{ GPa})/(13.2 \pm 1.5 \text{ GPa}) = 22.7 \pm 4.5$. Hence, within the experimental scatter, the indentation coefficient $\chi \propto (E/H)^{1/2}$ (Section II) may be considered essentially unchanged by addition of the second phase.

Accordingly, we may retain the calibrated parameters in Eq. (10) for our evaluations of the *normalized* T -curve in Eq. (1b) for the alumina-matrix composite material. Extension to evaluations of the *absolute* T -curve in Eq. (1a) is contingent on whether or not deflections along the interphase boundaries in the composite significantly alter the value of T_0 .

(6) T -Curve Constructions

The calibration from the previous subsection allows us to construct $T(c)$ diagrams for our materials from indentation-strength and in situ applied-stress/crack-size data.

We begin with the alumina control, as a check on the assumption $T = T_0$ implicit in Eqs. (5)–(7). The family of solid curves in Fig. 10 represents generations of the *normalized* function $K'_A(c)/T_0$ in Eq. (1b) (left ordinate) using inert strengths $\sigma_A = \sigma_M$ at each load P from Fig. 2, and corresponding *absolute* function $K'_A(c)$ in Eq. (1a) (right ordinate) assuming $T_0 = 2.75 \text{ MPa}\cdot\text{m}^{1/2}$ (grain boundary toughness¹⁶). The T -curve is the locus of tangency points to these curves, as defined by $dK'_A(c)/dc = dT(c)/dc$ in Eq. (4). This locus effectively coincides with the horizontal line $T(c) = T_0$, as required for a material with single-valued toughness. The individual points in Fig. 10 are similar generations of $K'_A(c)/T_0$ or $K'_A(c)$ from the in

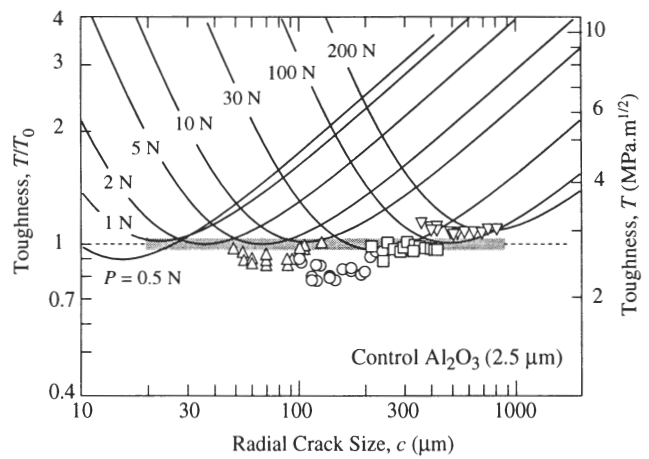


Fig. 10. T -curve diagram for fine-grain control alumina, grain size $2.5 \mu\text{m}$. Left axis normalized T/T_0 , right axis absolute T using $T_0 = 2.75 \text{ MPa}\cdot\text{m}^{1/2}$ as grain boundary toughness. Solid curves are plots of $K'_A(c)$ in Eq. (2) using alumina inert strengths σ_M at indentation loads P from Fig. 2. Data points are from in situ observations of $\sigma_A(c)$ in Fig. 5 at same loads. Shaded band is fitted T -curve at $T = T_0$.

situ $\sigma_A(c)$ data in Fig. 5. These points, representing equilibrium states in the growth evolution, are a *direct* measure of $T(c)$. Their tendency to fall below the dashed $T = T_0$ line may reflect the influence of slow crack growth, in addition to measurement uncertainties in the crack lengths. Notwithstanding such departures, the data substantiate the presumed invariance of toughness in the control alumina.

Figure 11 generates similar tangency constructions for the alumina test materials of grain sizes $15, 35,$ and $80 \mu\text{m}$ from the $\sigma_M(P)$ data sets in Fig. 3. Note that the $T(c)$ envelopes fall below the line $T = T_0$ at short crack sizes ($c < 400 \mu\text{m}$, approximately), and rise above this line at long crack sizes ($c > 400 \mu\text{m}$), reflecting the crossover in curves in Fig. 3. The steepness of the T -curve increases with grain size, again signifying a microstructural scaling effect in the shielding term. We note the absence of any firm indication that the toughness level has reached an upper plateau over the crack-size data range covered in these experiments.

Figure 12 is the T -curve construction for the alumina-matrix/aluminum titanate composite, generated from both inert strength (Fig. 4) and in situ (Fig. 9) data. Again, the data points from the in situ measurements are systematically displaced below and to the right of the $K'_A(c)$ inert-strength envelope, in keeping with the enhanced crack growth observed in this material. Nevertheless, the existence of a particularly steep T -curve for this material is manifest. An independent estimate of the long-crack toughness on a comparable composite material,³⁰ plotted as the upper dashed line at $T \approx 3T_0$ ($\approx 8 \text{ MPa}\cdot\text{m}^{1/2}$) in Fig. 12, signifies that the cumulative effect of bridging is incomplete over >2 mm crack growth in our experiments. We point out that a crack size of 2 mm represents an appreciable fraction of the thickness of the composite disks (5 mm) so, by virtue of specimen geometry effects in the K -field relations,⁶ any extrapolation of the data at extreme right in Fig. 12 becomes subject to considerable uncertainty.

V. Discussion

The present study offers an entirely objective strategy for evaluating short-crack T -curves from indentation-strength data. Underlying our evaluation for alumina-based ceramics is a proper calibration of the indentation-strength K -field coefficients for a fine-grain matrix material with negligible T -curve. With this calibration one may determine the T -curves from the K -field relation Eq. (2) in conjunction with the instability relation Eq. (4):^{1,33} (i) by generating families of $K'_A(c)$ curves for

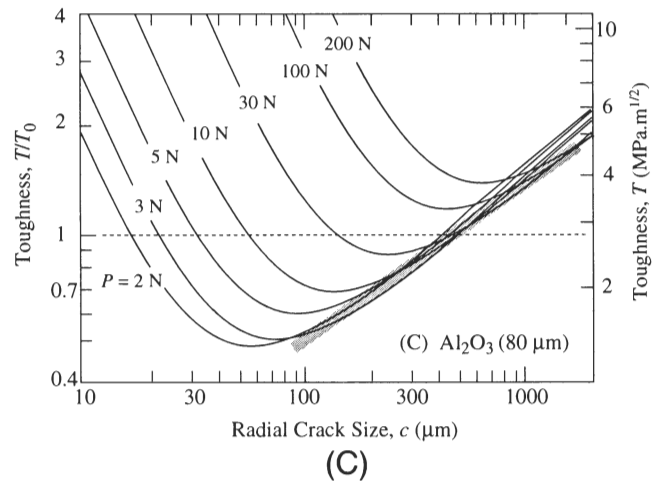
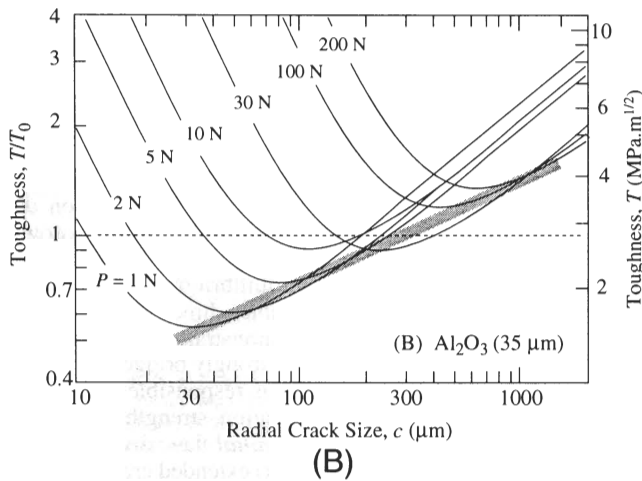
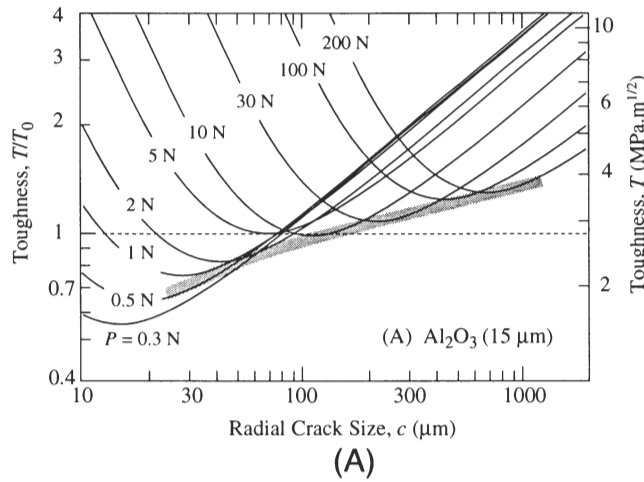


Fig. 11. T -curves for coarse-grain aluminas, grain sizes (A) 15, (B) 35, and (C) 80 μm . Left axis normalized T/T_0 , right axis absolute T using $T_0 = 2.75 \text{ MPa}\cdot\text{m}^{1/2}$ as grain boundary toughness. Solid curves are plots of $K'_A(c)$ in Eq. (2) using alumina inert strengths σ_M at indentation loads P from Fig. 3. Shaded bands are arbitrarily fitted T -curves.

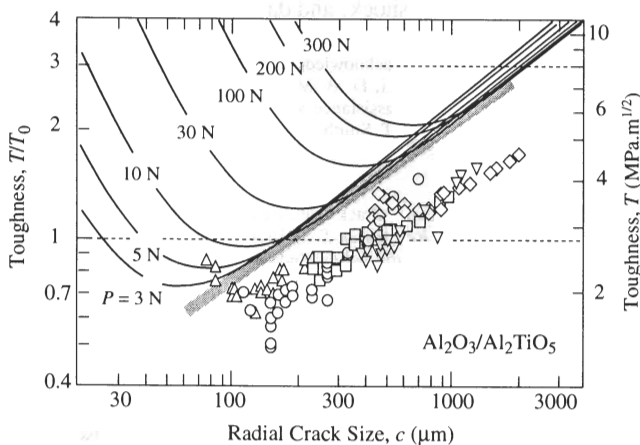


Fig. 12. T -curve for alumina-matrix/aluminum titanate composite. Left axis normalized T/T_0 , right axis absolute T using $T_0 = 2.75 \text{ MPa}\cdot\text{m}^{1/2}$ as grain boundary toughness. Solid curves are plots of $K'_A(c)$ in Eq. (2) using inert strengths σ_M at indentation loads P from Fig. 4. Data points are from in situ observations of $\sigma_A(c)$ at same loads. Upper horizontal dashed line is independent measurement of long-crack toughness using a compact tension specimen.³⁰ Shaded band is arbitrarily fitted T -curve.

inert strengths σ_M at given indentation loads P , and fitting an envelope of tangency points to these curves; (ii) by generating $K'_A(c)$ data sets directly from in situ $\sigma_A(c)$ data. The $T(c)$ evaluations are limited only by restrictions in the crack-size range over which the indentations remain well-behaved,²⁹ $\approx 50 \mu\text{m}$ to 2 mm in Figs. 10–12.

Our strategy removes all the objections to the indentation methodology stated in Section I. In situ observations confirm failures from indentation sites, with distinctive stable crack growth prior to failure, so the observed flaw tolerance evident for the materials in Figs. 3 and 4 cannot be dismissed as strength cutoffs from natural flaws. No preconceptions concerning the analytical form of $T(c)$ are implied in our evaluations. It is not even necessary to identify a priori specific shielding mechanisms. The key to our calibration of the indentation coefficients is the invariance of $\sigma_M P^{1/3}$ over the load range for the control material, as in the inert indentation–strength data for the fine-grain alumina in Fig. 2. This corresponds to an equivalent load invariance in the compound coefficient $\psi\chi^{1/3}$ in Eq. (6a), implying self similarity in the radial crack configurations at failure. *Within* this constraint, uncertainties in absolute determinations of the individual parameters ψ and χ simply compress or expand the $K'_A(c)$ curves in Fig. 10 along the c -axis, affecting the steepness but not the existence of the T -curve. *Without* this constraint, independent calibrations of ψ and χ can lead to artificial T -curves, even in materials like silicate glass where none exist.¹² Such inadmissible results have prompted some workers to adopt ad hoc calibration procedures:

e.g., fixing χ at its ideal theoretical value while force-fitting $\psi(c)$ to match the requirement $T = T_0$,^{6,12} or alternatively, fixing ψ while force-fitting $\chi(c)$.¹³ A predisposition of ψ and χ to dependency on c during the evolution to failure has been acknowledged in our present evaluations of the former coefficient from Eq. (10) for annealed indentations, as well as in evaluations from earlier studies.^{34,35} This potential complication is circumvented in the present procedure by the self similarity of the inert strength configurations implicit in Fig. 2.

The authenticity of the T -curves in Figs. 11 and 12 is supported by a weight of independent evidence. Experimental confirmation of a microstructural K -field shielding term, from frictional grain–grain bridging at the crack interface, has been documented in earlier microscopic studies on coarse aluminas and other ceramics.^{17,18} In addition, direct measurements of the crack-opening profiles indicate a strong closure effect from the bridging tractions.³⁶ The trend to a steepening T -curve with increasing grain size in Fig. 11 reflects that reported by Knehans and Steinbrech³⁷ for long-crack tests in alumina. This same trend was also noted in deconvolutions of the inert strength data in Fig. 11 using a grain bridging fracture mechanics model with several adjustable parameters.¹⁶ Quantitative comparisons with alternative T -curve evaluations are more tenuous, because of strong sensitivities to small errors in crack measurements (both technique- and material-related) and specimen geometry effects in the underlying fracture mechanics relations.

It is interesting to examine how the present calibration values of the K_A and K_R coefficients ψ and χ compare with previous estimates. Indentation flaws (and most natural flaws for that matter) tend to pennylike geometry.^{2,38} In the ideal case of a single embedded penny crack in an infinite solid with axial symmetry, $\psi = 2/\pi^{1/2} = 1.27$.² Vickers radial cracks, however, depart from such ideal geometry in several ways, all of which may be expected to affect ψ . They are characterized by mutual intersections with the specimen free surface and orthogonal radial and lateral crack systems.³⁸ They tend also to an elliptical front, the more so as they extend through a greater fraction of the specimen thickness, and are annular about the deformation zone rather than center-point loaded.⁸ For our as-indentated base alumina, with $T_0 = 2.75 \text{ MPa}\cdot\text{m}^{1/2}$ (Section IV(6)), Eq. (9b) yields $\psi = 0.77$. A determination from the strength/crack-size measurements on postindentation-annealed specimens using Eq. (10) in Section IV(3) gives $\psi = 0.96$ for the same alumina; an analogous determination from an earlier study on glass gave $\psi = 0.89$.³⁴ The lower value for as-indentated specimens is not inconsistent with a diminishing function $\psi(c)$ between c_0 and c_M .^{6,12,14,39} On the other hand, a previous calibration, using a “dummy” indentation technique to determine the critical crack size c_M on several ceramics and invoking $\sigma_M c_M^{1/2} = 3T_0/4\psi$ from Eq. (6),⁴⁰ gave $\psi = 1.24$.¹¹

Again using $T_0 = 2.75 \text{ MPa}\cdot\text{m}^{1/2}$ for our base alumina, Eq. (9a) yields $\chi = 0.076$. This value compares with $\chi = 0.071$ from measurements of immediate postindentation crack sizes in a fine-grain alumina,²⁹ but contrasts strongly with an earlier estimate $\chi = 0.018$ ¹¹ based on the dummy indentation method just mentioned (i.e., using $\psi = 1.24$ in Eq. (6a)). As with ψ , χ may be susceptible to relaxation with extending crack size. Also, in going from control material to test material, χ may be subject to variations from changes in indentation deformation, not least from changes in the modulus-to-hardness ratio, $\chi \propto (E/H)^{1/2}$ (Section II). This is not a factor in the “pure” aluminas, because changes in grain size have a negligible influence on the macroscopic elastic modulus and hardness of alumina. For aluminas with significant proportions of sintering additives, or alumina-based composites with additive second phases, changes in E and H will be the rule rather than the exception. In our aluminum titanate composite these changes are self-compensating, such that E/H , and presumably χ , remain unaltered (Section IV(5)). Very special caution needs to be exercised in those material systems in which the deformation in the second phase is not volume conserving, e.g., as with “anomalous

glasses”⁴¹ and phase-transforming zirconias,⁴² where the relation $\chi \propto (E/H)^{1/2}$ may be modified.²⁵

It is appropriate to weigh the advantages and limitations of the two variants of the indentation methodology advocated here for evaluating T -curves. Consider first the *indentation–strength* route, based on $\sigma_M(P)$ data for both test and control materials. The procedure is routine, fast, and free of potential complications from slow crack growth. However, several specimens (typically, a minimum of four) are required at each load over a wide range of indentation loads to generate an adequate data set. In addition, a complete calibration of the indentation coefficients requires some measurements of critical crack sizes, $c_M(P)$, on a representative number of control specimens. Here in situ observations on fine-grain alumina were used (Figs. 4 and 5) to determine $c_M(P)$. In principle, one could use the simpler “dummy” indentation technique^{6,40} to measure c_M values, but at considerable potential sacrifice in certainty.⁴⁰

With the alternative route, the roles are reversed. In situ, $\sigma_A(c)$ measurements on the actual test specimens then constitute the core of the T -curve evaluation—inert-strength data are needed only on the control material. From a quantitative standpoint, this route is not so practical for those materials that do not form well-defined indentation patterns, such as our coarsest-grain aluminas (Section IV(4)). Also, as noted for the composite material in Fig. 12 (and to a lesser extent for the control alumina in Fig. 10), the data are susceptible to slow crack growth. In relation to Eq. (2), such enhanced extension displaces the data to the right (enhanced crack size c) and downward (diminished K'_A at prescribed applied stress σ_A and indentation load P) relative to the equilibrium T -curve. On the other hand, the in situ procedure enables direct confirmation of failure from the indentations, and demonstrates enhancement of precursor stable growth in the more strongly bridged materials. It is this enhanced stabilization that is responsible for the flaw tolerance demonstrated in indentation–strength tests: the strength is no longer dependent on *initial* flaw size, but rather on some critical (history-independent) extended crack length to an instability (tangency) configuration.^{10,15,16,31} The K_R -field from the residual contact stresses in as-indentated specimens augments this stability, and thereby extends the range of crack sizes over which useful $T(c)$ data may be accumulated. Finally, in situ observations are able to provide clues to the underlying microstructural shielding processes (in our case, bridging) responsible for the T -curve behavior.

The indentation methodology proposed here for evaluating toughness properties of ceramics is pertinent to short-crack properties, clearly to *strength* but also to spontaneous microcracking, wear, thermal shock, and damage accumulation.

Acknowledgments: We acknowledge stimulating discussions with R. F. Cook, E. R. Fuller, Jr., C. W. Li, D. B. Marshall, N. P. Padture, R. O. Scattergood and S. M. Smith, and assistance with the design of the in situ crack growth device in Fig. 1 from D. T. Smith.

References

1. W. Mai and B. R. Lawn, “Crack Stability and Toughness Characteristics in Brittle Materials,” *Annu. Rev. Mater. Sci.*, **16**, 415–39 (1986).
2. B. R. Lawn, *Fracture of Brittle Solids*, 2nd ed. Cambridge University Press, Cambridge, U.K., in press.
3. D. J. Green, R. H. J. Hannink, and M. V. Swain, *Transformation Toughening of Ceramics*. CRC Press, Boca Raton, FL, 1989.
4. D. B. Marshall, “Strength Characteristics of Transformation-Toughened Zirconia,” *J. Am. Ceram. Soc.*, **69** [3] 173–80 (1986).
5. R. W. Steinbrech and O. Schmenkel, “Crack Resistance Curves of Surface Cracks in Alumina,” *J. Am. Ceram. Soc.*, **71** [5] C-271–C-273 (1988).
6. N. Ramachandran and D. K. Shetty, “Rising Crack-Growth-Resistance (R -Curve) Behavior of Toughened Alumina and Silicon Nitride,” *J. Am. Ceram. Soc.*, **74** [10] 2634–41 (1991).
7. T. Fett and D. Munz, “Evaluation of R -curves in Ceramic Materials Based on Bridging Interactions,” Report of the Nuclear Research Center Karlsruhe, Karlsruhe, Germany, 1991.
8. D. B. Marshall, B. R. Lawn, and P. Chantikul, “Residual Stress Effects in Sharp-Contact Cracking: II. Strength Degradation,” *J. Mater. Sci.*, **14** [9] 2225–35 (1979).
9. R. F. Cook and B. R. Lawn, “Controlled Indentation Flaws for Construction of Toughness and Fatigue Master Maps,” pp. 22–42 in ASTM Special Technical

Publication No. 844, *Methods for Assessing the Structural Reliability of Brittle Materials*. Edited by S. W. Freiman and C. M. Hudson. American Society for Testing and Materials, Philadelphia, PA, 1984.

¹⁰R. F. Cook, B. R. Lawn, and C. J. Fairbanks, "Microstructure-Strength Properties in Ceramics: I, Effect of Crack Size on Toughness," *J. Am. Ceram. Soc.*, **68** [11] 604-15 (1985).

¹¹R. F. Cook, C. J. Fairbanks, B. R. Lawn, and Y.-W. Mai, "Crack Resistance by Interfacial Bridging: Its Role in Determining Strength Characteristics," *J. Mater. Res.*, **2** [3] 345-56 (1987).

¹²S. M. Smith and R. O. Scattergood, "Crack Shape Effects in Fracture Toughness Measurements," *J. Am. Ceram. Soc.*, **75** [2] 305-15 (1992).

¹³C.-W. Li, D.-J. Lee, and S.-C. Lui, "R-Curve Behavior and Strength of In-Situ Reinforced Silicon Nitrides with Different Microstructures," *J. Am. Ceram. Soc.*, **75** [7] 1777-85 (1992).

¹⁴R. M. Anderson and L. M. Braun, "Technique for the R-Curve Determination of Y-TZP Using Indentation-Produced Flaws," *J. Am. Ceram. Soc.*, **73** [10] 3059-62 (1990).

¹⁵Y.-W. Mai and B. R. Lawn, "Crack-Interface Grain Bridging as a Fracture Resistance Mechanism in Ceramics: II, Theoretical Fracture Mechanics," *J. Am. Ceram. Soc.*, **70** [4] 289-94 (1987).

¹⁶S. J. Bennison and B. R. Lawn, "Role of Interfacial Grain-Bridging Sliding Friction in the Crack-Resistance and Strength Properties of Nontransforming Ceramics," *Acta Metall.*, **37** [10] 2659-71 (1989).

¹⁷P. L. Swanson, C. J. Fairbanks, B. R. Lawn, Y.-W. Mai, and B. J. Hockey, "Crack-Interface Grain Bridging as a Fracture Resistance Mechanism in Ceramics: I, Experimental Study on Alumina," *J. Am. Ceram. Soc.*, **70** [4] 279-89 (1987).

¹⁸P. L. Swanson, "Crack-Interface Traction: A Fracture-Resistance Mechanism in Brittle Polycrystals"; pp. 135-55 in *Advances in Ceramics*, Vol. 22, *Fractography of Glasses and Ceramics*. American Ceramic Society, Columbus, OH, 1988.

¹⁹R. F. Krause, "Rising Fracture Toughness from the Bending Strength of Indented Alumina Beams," *J. Am. Ceram. Soc.*, **71** [5] 338-43 (1988).

²⁰R. F. Cook and D. R. Clarke, "Fracture Stability, R-Curves and Strength Variability," *Acta Metall.*, **36** [3] 555-62 (1988).

²¹D. K. Shetty and J. S. Wang, "Crack Stability and Strength Distribution of Ceramics That Exhibit Rising Crack-Growth (R-Curve) Behavior," *J. Am. Ceram. Soc.*, **72** [7] 1158-62 (1989).

²²P. Chantikul, S. J. Bennison, and B. R. Lawn, "Role of Grain Size in the Strength and R-Curve Properties of Alumina," *J. Am. Ceram. Soc.*, **73** [8] 2419-27 (1990).

²³S. J. Bennison, N. P. Padture, J. L. Runyan, and B. R. Lawn, "Flaw-Insensitive Ceramics," *Philos. Mag. Lett.*, **64** [4] 191-95 (1991).

²⁴D. B. Marshall and B. R. Lawn, "Residual Stress Effects in Sharp-Contact Cracking: I. Indentation Fracture Mechanics," *J. Mater. Sci.*, **14** [8] 2001-12 (1979).

²⁵B. R. Lawn, A. G. Evans, and D. B. Marshall, "Elastic/Plastic Indentation Damage in Ceramics: The Median/Radial Crack System," *J. Am. Ceram. Soc.*, **63** [9-10] 574-81 (1980).

²⁶J. L. Runyan and S. J. Bennison, "Fabrication of Flaw-Tolerant Aluminum-Titanate-Reinforced Alumina," *J. Eur. Ceram. Soc.*, **7**, 93-99 (1991).

²⁷N. P. Padture, S. J. Bennison, and H. M. Chan, "Flaw Tolerance and Crack Resistance Properties of Alumina-Aluminum Titanate Composites with Tailored Microstructures," *J. Am. Ceram. Soc.*, in review.

²⁸D. B. Marshall, "An Improved Biaxial Flexure Test for Ceramics," *Am. Ceram. Soc. Bull.*, **59** [5] 551-53 (1980).

²⁹G. R. Anstis, P. Chantikul, B. R. Lawn, and D. B. Marshall, "A Critical Evaluation of Indentation Techniques for Measuring Fracture Toughness: I, Direct Crack Measurements; II, Strength Method," *J. Am. Ceram. Soc.*, **64** [9] 533-38, 539-43 (1981).

³⁰N. P. Padture, "Crack Resistance and Strength Properties of Some Alumina-Based Ceramics with Tailored Microstructures"; Ph.D. Thesis. Lehigh University, Bethlehem, PA, 1991.

³¹S. J. Bennison, J. Rödel, S. Lathabai, P. Chantikul, and B. R. Lawn, "Microstructure, Toughness-Curves and Mechanical Properties of Alumina Ceramics"; pp. 209-33 in *Toughening Mechanisms in Quasi-Brittle Materials*. Edited by S. P. Shah. Kluwer Academic Publishers, Dordrecht, The Netherlands, 1991.

³²D. B. Marshall, "Controlled Flaws in Ceramics: A Comparison of Knoop and Vickers Indentation," *J. Am. Ceram. Soc.*, **66** [2] 127-31 (1983).

³³R. F. Cook, "Segregation Effects in the Fracture of Brittle Materials: Ca-Al₂O₃," *Acta Metall.*, **38** [6] 1083-100 (1990).

³⁴D. B. Marshall and B. R. Lawn, "Flaw Characteristics in Dynamic Fatigue," *J. Am. Ceram. Soc.*, **63** [9-10] 532-36 (1980).

³⁵B. R. Lawn, K. Jakus, and A. C. Gonzalez, "Sharp vs Blunt Crack Hypothesis in the Strength of Glass," *J. Am. Ceram. Soc.*, **68** [1] 25-34 (1985).

³⁶J. Rödel, J. Kelly, and B. R. Lawn, "In Situ Measurements of Bridged Crack Interfaces in the SEM," *J. Am. Ceram. Soc.*, **73** [11] 3313-18 (1990).

³⁷R. Knehans and R. Steinbrech, "Effect of Grain Size on the Crack Resistance Curves of Al₂O₃ Bend Specimens," *Sci. Ceram.*, **12**, 613-19 (1983).

³⁸B. R. Lawn and T. R. Wilshaw, "Indentation Fracture: Principles and Applications," *J. Mater. Sci.*, **10** [6] 1049-81 (1975).

³⁹R. Steinbrech, "Growth of Indentation Cracks in Al₂O₃ under Loading"; presented at the European Ceramic Society, Augsburg, FRG, 1991.

⁴⁰R. F. Cook and B. R. Lawn, "A Modified Indentation Toughness Technique," *J. Am. Ceram. Soc.*, **66** [11] C-200-C-201 (1983).

⁴¹A. Arora, D. B. Marshall, B. R. Lawn, and M. V. Swain, "Indentation Deformation/Fracture of Normal and Anomalous Glasses," *J. Non-Cryst. Solids*, **31** [3] 415-28 (1979).

⁴²R. F. Cook and L. M. Braun, "Trapped Cracks at Indentations: I. Experiments on Y-TZP; II. Fracture Mechanics Model," *J. Mater. Res.*, to be submitted. □